CEAS Aeronautical Journal (2024) 15:529–543
https://doi.org/10.1007/s13272-023-00675-w

ORIGINAL PAPER

# A multi-model and multi-objective approach to the design of helicopter flight control laws

**Patrick Authié**[1]

Received: 16 March 2023 / Revised: 11 June 2023 / Accepted: 26 June 2023 / Published online: 6 July 2023


**Abstract**
This study addresses the design of a full-authority Attitude Command-Attitude Hold flight control system for the Bo-105 helicopter. A single sixth-order dynamic controller replaces the PID-based arrangement that usually forms the core of rotorcraft flight control systems. The proposed design methodology combines multi-model and multi-objective approaches within the framework of structured $H_\infty$ software tools. Owing to the multi-model approach, only two sets of gains are sufficient to cover the entire speed range between hover and maximum velocity. In addition, $\mu$-analysis tools can be used in conjunction with this approach to improve robustness against parametric uncertainties. Simultaneously, the multi-objective approach facilitates the design process and establishes connections between the tuning parameters and handling qualities. The performance of the resulting flight control system is investigated in this study, and evaluated against the attitude quickness, bandwidth and inter-axis coupling criteria, as defined by ADS-33. The resulting design achieves Level 1 performance in most cases. Besides, the merits and limitations of the proposed methodology are discussed in this paper.

**Keyword** Multi-model and multi-objective design, Helicopter flight controls, Dynamic controller, Handling qualities objectives

## 1 Introduction

Owing to the natural instability of a rotorcraft, flying a helicopter without artificial stability augmentation or a full-authority flight control system is extremely difficult. Stiles et al. consider that the advantages of rotorcraft fly-by-wire technology make it "impossible to resist" [1]. However, the complex dynamics and inter-axis coupling involved in helicopter flight render the development of flight control laws a serious technical challenge. Over the past decades, several different techniques have been investigated to address this issue [2] and enhance rotorcraft handling qualities (HQ), the desirable characteristics of which are specified in standards such as ADS-33E-PRF [3]. Notably, despite the availability of numerous modern control techniques, classical PID controllers continue to be used in existing helicopter flight control systems.

Another difficulty in the design of flight control laws may arise from the lack of direct connection between the ADS-33 HQ criteria and the design procedures that rely on the different available control techniques. Researches have been conducted under the auspices of NASA to consider HQ requirements at the early design stage. These studies have led to the development of the CONDUIT software tool [4]. In Europe, recent studies at ONERA [5–7] have resulted in the development of an approach aimed at integrating HQ objectives into robust PID control design techniques [8]. The authors developed a PID-based Attitude Command-Attitude Hold (ACAH) controller for a rigid-body model of the EC-225 using a multi-objective and multi-model design approach. The primary objectives of the study were to follow a reference model on each axis and minimise actuator activity. The gains were first designed for a single model representing the helicopter dynamics in hover. In the second step, the multi-model approach considered multiple models addressing various weight and balance configurations, at speeds ranging from 0 to 40 knots. The resulting controllers were evaluated based on the ADS-33 bandwidth, attitude quickness and oscillatory-mode damping criteria.

✉ Patrick Authié
patrick.authie@dbmail.com

[1] Chaville, France

In this study, an ACAH flight control system for the Bo-105 helicopter was developed based on a comparable multi-objective and multi-model approach. Reference models are also used to enforce HQ objectives; however, the presented design methodology introduces several new aspects. In addition to rigid-body dynamics, the design model entails rotor effects, computational delay, roll-off filters, and actuator and sensor dynamics. Furthermore, the three PIDs are replaced by a single sixth-order dynamic controller that considers the collective input. Additional design objectives were established, such as the maximum relative matching error between the reference models and the actual system response, minimum stability margins, and minimisation of the disturbances induced by the collective input on the three remaining axes. The multi-model approach was used to synthesise two sets of controller gains. The first addresses speeds from hover to 70 kts, and the second addresses speeds from 70 kts up to maximum velocity. Furthermore, this approach was combined with structured singular value (SSV) analysis to enhance the robustness of the design against parametric uncertainties.

The remainder of this paper is organised as follows. Section 2 introduces the helicopter model, and closed-loop and controller architectures. Section 3 details the design methodology; in particular, it describes how the multi-objective and multi-model approaches were implemented. Section 4 analyses the performance of the resulting design in both the time and frequency domains. The conclusions are presented in Sect. 5.

## 2 Design model

This section describes the general framework used in the design. First, the modelling of the helicopter is detailed, followed by the closed-loop architecture, and, finally, the controller architecture, which is one of the most salient features of this study.

### 2.1 Bo-105 helicopter model

The Bo-105 helicopter was selected for the present study because of its strong inter-axis coupling, which poses a significant challenge in the design of control laws. An analysis of the Bo-105 bare airframe dynamics [9] shows that the pitch to roll coupling is on the Level 2 to Level 3 boundary according to the criterion defined by ADS-33. The helicopter dynamics are represented in the design process by a linear time-invariant model using the standard form, which is given by Eq. (1).

$$\begin{cases} \dot{X} = A\,X + B\,u \\ Y = C\,X \end{cases} \tag{1}$$

where X is the state vector and $u = [\delta_{lon}\ \delta_{lat}\ \delta_{ped}\ \delta_{col}]^T$ is the control input. Vector $u$ entails the longitudinal, lateral, tail rotor, and collective inputs in that order. A, B, and C are the stability, control, and output matrices, respectively. The measurement vector Y comprises the measurements of the attitude angles ($\theta, \varphi, \psi$) and body-axis angular velocities (q, p, r). The model-building process begins with a set of matrices obtained at eight different trim velocities, from hover up to 140 kts, with a 20 kts increment [10]. These matrices represent the 6 degrees of freedom rigid-body dynamics of the aircraft.

In the second step, the eight models are augmented to consider rotor effects. First-order models are used to simulate the main rotor lag effects, as described in Appendix C of Srinathkumar's book [11]. The inflows of the main and tail rotors are also represented by first-order models whose time constants are set to 0.8 s and 0.15 s, respectively. This augmentation eventually leads to the attainment of 13th-order helicopter models.

The third and last step entails using the eight linearised models to generate a single quasi-linear parameter-varying (qLPV) model that represents the aircraft dynamics continuously between 0 and 140 kts. This is achieved by means of polynomial regressions. With this approach, matrices A and B in Eq. (1) become functions of the longitudinal airspeed, denoted by $u$. Let $a_{ij}$ and $b_{ij}$ denote the elements present at the $i^{th}$ row and $j^{th}$ column of matrices A and B, respectively. Then, $a_{ij}(u) = \sum_{k=0}^{n} \alpha_{ijk}.u^k$ and $b_{ij}(u) = \sum_{k=0}^{n} \beta_{ijk}.u^k$, where $\alpha_{ijk}$ and $\beta_{ijk}$ are the polynomial coefficients to be found. In this study, the coefficients $\alpha_{ijk}$ and $\beta_{ijk}$ were obtained using polynomial regressions of degree $n = 4$.

### 2.2 Design model architecture

Figure 1 presents the design model, which has three inputs: the pitch, roll, and yaw angle references. These are denoted by $\theta_{ref}$, $\varphi_{ref}$ and $\psi_{ref}$, respectively. The tracking errors $e_\theta$, $e_\varphi$, and $e_\psi$ are integrated, and the error integrals $I_\theta$, $I_\varphi$, and $I_\psi$ are sent to the controller, which also takes the measurement vector Y and collective pitch $\delta_{col}$ as inputs. However, the collective is excluded from the closed-loop scheme, and the vector $U_{cmd}$ issued by the controller comprises pitch, roll and yaw commands, which are denoted as $\delta_\theta$, $\delta_\varphi$, and $\delta_\psi$, respectively.

The helicopter plant is the most important component of the global design model. However, other elements may have a significant influence on the closed-loop behaviour. Therefore, the design model includes sensor and actuator models. They are represented by first-order transfer functions, the time constants of which are set to 80 ms for the sensors and 16 ms for the actuators. In addition,

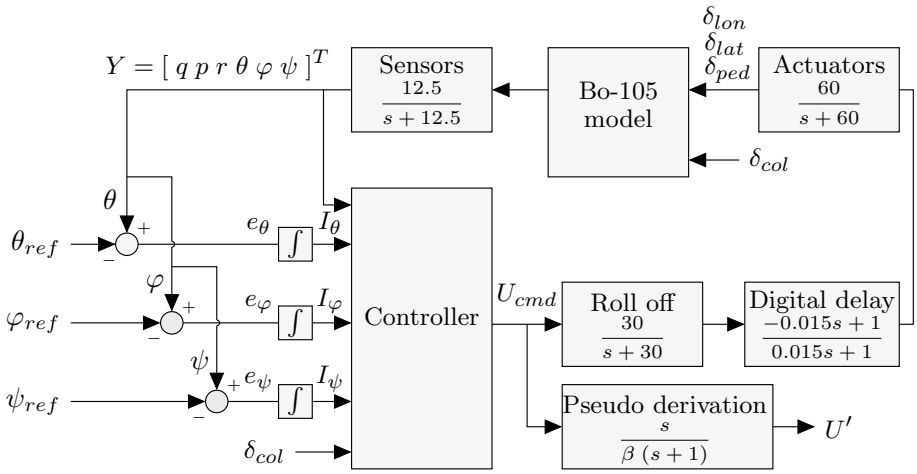


**Fig. 1** ACAH system design model

a computational delay of 30 ms is simulated using first-order Padé filters, and the closed loop is fitted with roll-off filters on the pitch, roll and yaw axes, as shown in Fig. 1. The open-loop scheme, which includes the roll-off filters, delay, plant, and actuator and sensor models, has 28 states. Figure 1 also shows a pseudo-derivative filter that uses the command vector $U_{cmd}$ issued by the controller as the input. This filter is not included in the closed-loop scheme. Instead, it is used for design purposes, as detailed in the next section. The transfer $T_{U_{cmd}\to U'}$ between the input $U_{cmd} = [\delta_\theta\ \delta_\varphi\ \delta_\psi]^T$ and output $U' = [\delta'_\theta\ \delta'_\varphi\ \delta'_\psi]^T$ is given by Eq. (2).

$$T_{U_{cmd}\to U'}(s) = \frac{s}{\beta\ (s+1)} \times I_3 \tag{2}$$

where $\beta$ is a scalar design parameter and $I_3$ is the $3 \times 3$ identity matrix.

### 2.3 Dynamic controller

Conventional ACAH flight control systems embed one PID controller per axis of the closed loop. In the present study, the PIDs were replaced by a single sixth-order dynamic controller. One advantage of this design over the usual arrangement is that the controller can be designed to consider inter-axis couplings, which dispenses with the use of channel interconnections to mitigate undesired cross-couplings. The order of the controller was determined after successive trials in which the controller order was increased incrementally. These trials revealed that the performance of the controller increased until order 6, before decreasing for higher order systems. The dynamics of the controller are driven by the linear system in Eq. (3).

$$\begin{cases} \dot{X}_c = A_c\ X_c + B_c\ Y_c \\ U_{cmd} = C_c\ X_c + D_c\ Y_c \end{cases} \tag{3}$$

where $X_c$ is the six-vector of the controller internal states and $Y_c = [\ q\ p\ r\ \theta\ \varphi\ \psi\ I_\theta\ I_\varphi\ I_\psi\ \delta_{col}]^T$ is the input vector. The controller synthesis entails finding matrices $A_c$, $B_c$, $C_c$ and $D_c$. In the present study, one set of matrices addresses the 0–70 kts speed range, and the second set addresses the upper half of the flight envelope (70–140 kts).

## 3 Design methodology

The design of the proposed system uses the multi-model and multi-objective capabilities of the MATLAB systune function. The first two subsections introduce the multi-model and multi-objective approaches, and the third subsection details the practical implementation of the design methodology.

### 3.1 Multi-model approach

As mentioned earlier, two sets of gain matrices were designed, and each of which addresses one half of the speed range. In a previous study by Biannic et al. [8], multiple models were considered simultaneously for the design of PID gains. These models were included in a linear fractional representation, which was handled by the systune function as a single uncertain model. However, the systune function can explicitly consider multiple models simultaneously. In the present study, the low-speed matrices were thus computed against 71 linearised models, representing the helicopter dynamics between 0 and 70 kts with a 1 kt step. These linear models were obtained using the qLPV system described in the previous section. Similarly, the high-speed matrices were synthetised considering 71 models between 70 and 140 kts. The other components of the closed loop remained unchanged throughout the

speed range. With this methodology, almost every point in the flight envelope becomes a design point. One advantage of this method is that interpolation of the gain matrices is not required to cover the entire flight envelope. Instead, the gain matrices are switched when the airspeed crosses the 70 kts threshold. The multi-model approach can also be used to increase the robustness of the design, as shown in subsection 3.3.2.

## 3.2 Multi-objective approach

In addition to the array of closed-loop models, the systune function takes a list of design objectives as an input argument, which are referred to as "tuning goals". Subsequently, the systune function is applied to find a set of matrices that meet these objectives for all 71 models being considered.

The tuning goals can be labelled by the user as either "hard" or "soft". Hard goals have the highest priority. In contrast, soft goals are secondary objectives which systune attempts to satisfy subject to the constraint that hard goals have been attained. In addition to the controller gains, systune returns two scalar values, denoted by $\gamma_H$ and $\gamma_S$, which indicate whether the goals are satisfied by the computed controller. $\gamma_H \leq 1$ ($\gamma_S \leq 1$) means that all hard (soft) goals could be satisfied. In contrast, a returned value greater than one indicates that systune failed to enforce at least one goal. In this study, three tuning goals were specified in both the time and frequency domains for the design of the proposed flight control system.

### 3.2.1 Step tracking

In the present study, Step Tracking was defined as a hard goal. This tuning goal forces the responses of the attitude angles to match those of reference models within a specified tolerance. One advantage of using reference models is that they can be selected based on whether they meet HQ objectives, which are defined using the ADS-33 criteria. Three reference models, $R_\theta$, $R_\varphi$ and $R_\psi$ were defined for the pitch, roll, and yaw axes, respectively. These models were built as the product of a second-order transfer function and a first-order function, as shown in Eq. (4).

$$R_{\theta,\varphi,\psi}(s) = \frac{{\omega^2}_{\theta,\varphi,\psi}}{s^2 + 2\,\zeta\,\omega_{\theta,\varphi,\psi}\,s + {\omega^2}_{\theta,\varphi,\psi}} \times \frac{1}{0.1s+1} \tag{4}$$

The time response of the reference model is mainly driven by the second-order function. The purpose of the first-order function is to make the tracking requirement easier to satisfy for systune, while having limited influence on the reference model time response. The damping ratio $\zeta$ was set to 0.7 for the three reference models. The natural frequencies were selected to meet Level 1 performance according to the ADS-33 bandwidth criterion ("All other MTEs" - Usable Cue Environment (UCE) > 1 and/or Divided Attention operations). Therefore, the values of $\omega_\theta$, $\omega_\varphi$ and $\omega_\psi$ were set to 2, 4, and 2.5 rad/s, respectively. Consequently, the pitch and roll axes can be predicted to exhibit Level 1 performance with respect to the attitude quickness criterion, whereas the yaw axis will be limited to Level 2. Reaching Level 1 would have required the use of a higher frequency for the yaw-axis reference model; however, this higher frequency would have led to excessive actuator activity and potential saturation. Therefore, a compromise must be made in the design.

### 3.2.2 Margins

This tuning goal specifies minimum stability margins objectives. In this study, the Margins goal was defined as hard. The stability objectives are expressed in terms of disk-based margins [12], which provide more reliable estimates of stability than classical gain and phase margins. One advantage of disk-based margins is that simultaneous gain and phase variations are considered, whereas classical margins consider either gain or phase variation, but not both.

Figure 2 illustrates the difference between the classical and disk-based margins. Consider a multiplicative complex perturbation $f$ inserted into the loop under investigation. The closed loop will remain stable for any perturbation $f$ belonging to the union of the arc of the unit circle defined by the classical phase margin $\phi_c$, and a segment of the real axis bounded by the lower and upper classical gain margins ($g_{min}$ and $g_{max}$). Stability is not guaranteed outside this domain. Simultaneous gain and phase variations are therefore not covered by the classical margins.

In contrast, the disk margins provide a two-dimensional guaranteed stability domain. Closed-loop stability is retained for any complex perturbation $f$ lying within the disk defined

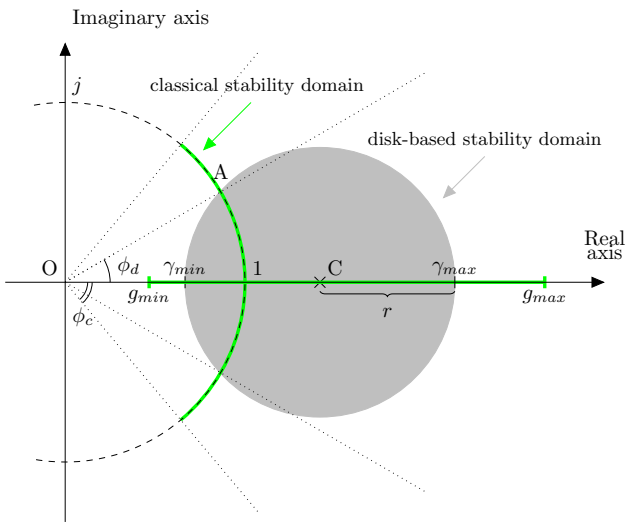


**Fig. 2** Guaranteed stability domains using classical and disk-based margins

by the phase-only disk margin $\phi_d$ and the gain-only disk margins ($\gamma_{min}, \gamma_{max}$). The phase-only and gain-only disk margins are more conservative than their classical counterparts:

$$\begin{cases} \gamma_{min} \geq g_{min} \\ \gamma_{max} \leq g_{max} \\ \phi_d \leq \phi_c \end{cases} \tag{5}$$

The systune function considers the so-called "balanced case", for which $\gamma_{max} = {\gamma_{min}}^{-1} = \gamma$. This means that the gain can increase or decrease by the same factor without causing unstability. In this study, the disk margin objectives $\gamma$ and $\phi_d$ were set to 2 (i.e. ± 6 dB) and ± 45º, respectively.

#### 3.2.3 Gain

The objective of this tuning goal is to force the gain $T_{i\to o}(s)$ from a specified input $i$ to a specified output $o$ to remain below a defined frequency-dependent value $W(s)$. This approach builds on the $H_\infty$ loop-shaping methodology, which uses weighting functions to shape the closed-loop response. Furthermore, systune relies heavily on the structured $H_\infty$ theory, and utilises nonsmooth optimisation techniques to minimise $H_\infty$ norms [13–16]. For the Gain goal, the function adjusts the tunable parameters of the system to minimise the $H_\infty$ norm $\| W_F(s)T_{i\to o}(s,x) \|_\infty$, where $W_F$ is the regularized gain profile derived from $W$, and $x$ is the vector of tunable parameters. In this study, $x$ gathers the 144 tunable elements of matrices $A_c$, $B_c$, $C_c$ and $D_c$ in Eq. (3), and the Gain goal was used as follows:

- The transfers between the collective input and tracking errors, denoted as $T_{\delta_{col}\to e_\theta}$, $T_{\delta_{col}\to e_\varphi}$ and $T_{\delta_{col}\to e_\psi}$, must remain below the frequency profile $W_1$. This was intended to mitigate the disturbance induced by the collective input on the pitch, roll and yaw channels. In the present study, this goal was defined as hard.
- Profile $W_2$ defines the maximum values of the transfers between the angular references and output of the pseudo-derivative filter shown in Fig. 1. These transfers are denoted as $T_{\theta_{ref}\to\delta'_\theta}$, $T_{\varphi_{ref}\to\delta'_\varphi}$ and $T_{\psi_{ref}\to\delta'_\psi}$. In what follows, parameter $\beta$ in Eq. (2) was set to 0.71. $W_2$ also limits the transfers between the collective input and pseudo-derivative filter output, denoted as $T_{\delta_{col}\to\delta'_\theta}$, $T_{\delta_{col}\to\delta'_\varphi}$ and $T_{\delta_{col}\to\delta'_\psi}$. The profile forces the transfers to roll off beyond 10 rad/s. Its purpose is to limit actuator activity in the medium–high frequency range, which not only increases the closed-loop robustness, but also helps avoid actuator saturation. This goal was defined as hard.
- Profile $W_3$ limits the transfers between the references and controller output in the 2–30 rad/s frequency range. These transfers are denoted as $T_{\theta_{ref}\to\delta_\theta}$, $T_{\varphi_{ref}\to\delta_\varphi}$ and $T_{\psi_{ref}\to\delta_\psi}$. The objective of $W_3$ is to limit actuator activity, which is complementary to the previous goal. Therefore, it was defined as a soft objective. Figure 3 shows gain profiles $W_1$, $W_2$ and $W_3$.

### 3.3 Practical implementation of the methodology

Once the tuning goals introduced in the previous subsection were selected, both sets of matrices were designed following a two-step procedure.

#### 3.3.1 First step: initial design

The first step begins with the invocation of the systune function. As mentioned previously, the function is required to find a set of matrices that meet the list of tuning objectives for 71 design models. An inspection of the $\gamma_H$ and $\gamma_S$ parameters returned by the function indicates whether the constraints are satisfied. Table 1 lists these parameters for both the low- and high-speed controllers after the first call to the function. In both scenarios, $\gamma_H$ is lower than but almost equal to 1. This

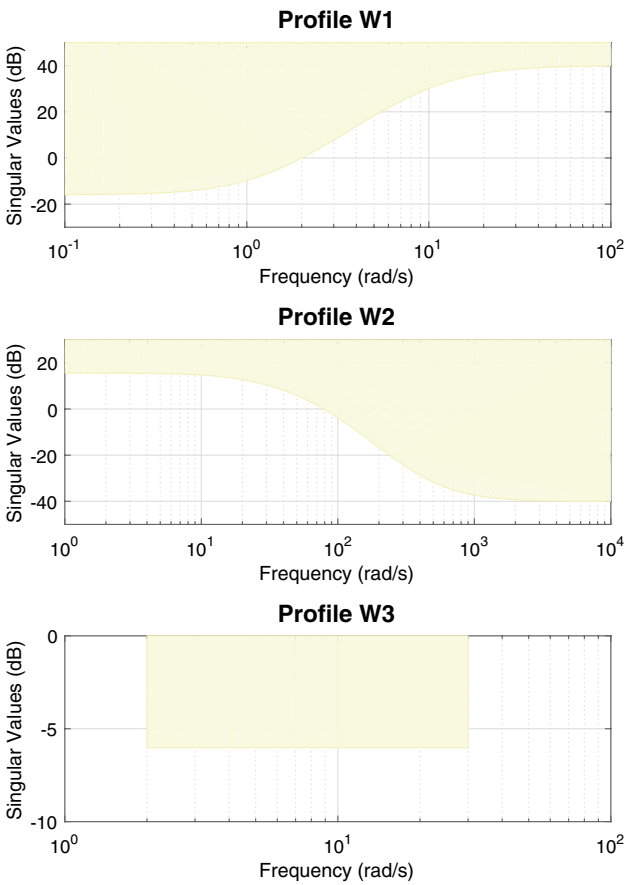


**Fig. 3** Gain profiles $W_1$, $W_2$ and $W_3$

**Table 1** $\gamma_H$ and $\gamma_S$ after the first call

| Speed range (kts) | $\gamma_H$ | $\gamma_S$ |
|---|---|---|
| 0-70 | 0.999 | 2.543 |
| 70-140 | 0.9991 | 1.8175 |

indicates that the systune function just fulfilled the minimum hard requirements; thus, the remaining degrees of freedom could be dedicated to meeting the soft objective. However, the latter could not be satisfied, as indicated by $\gamma_S$, which is greater than 1 in both cases. Nevertheless, this combination (i.e. $\gamma_H \leq 1$ and $\gamma_S > 1$) proves that the optimisation capabilities of the systune function have been fully leveraged. Fulfilling the soft objective as well would have indicated that the systune function could have enforced more demanding requirements. Subsequently, the robustness of the resulting controllers is assessed using SSV analysis. To this end, a qLPV uncertain model of the helicopter was derived from the design model by defining a $\pm$ 20% uncertainty for all stability and control derivatives in matrices A and B of Eq. (1), except for the vertical force due to pitch rate $z_q$ and the side force due to yaw rate $y_r$. These two parameters, in their concise form and in absolute terms, are approximately equal to airspeed, for which an absolute uncertainty of $\pm$ 1 kt is employed throughout the flight envelope. The lower and upper bounds of the SSV (also referred to as $\mu$) are then plotted for the median

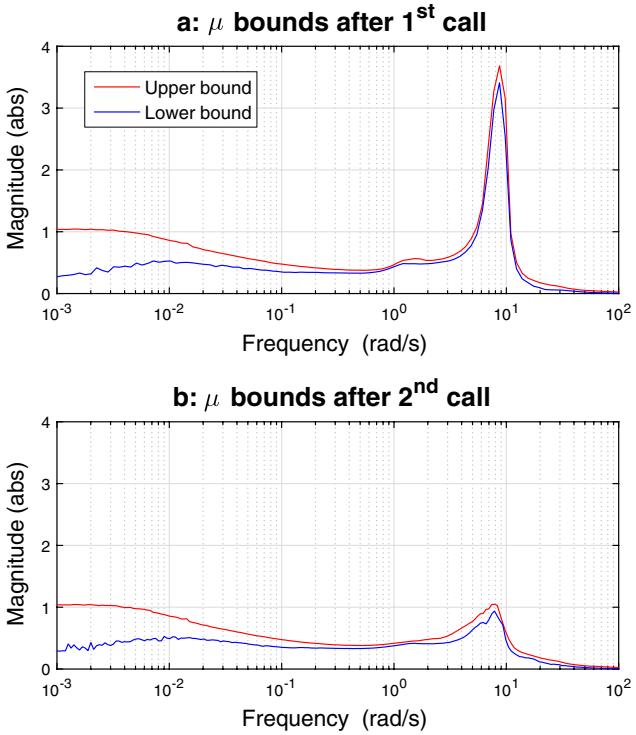


**Fig. 4** Structured singular value analysis at 35 kts

speed of each half of the flight envelope (i.e. 35 and 105 kts). Figure 4a shows the plots for the 35 kts uncertain model in closed loop with the roll-off filters, digital delay, actuator and sensor models, and the low-speed controller obtained after the first call to systune. Both the upper and lower bounds peak at approximately 3.5, indicating that robust stability is guaranteed for only 100 / 3.5 = 28.5% of the specified uncertainty. This figure is 49% at 105 kts.

### 3.3.2 Second step: robustness improvement

The second step of the methodology comprises enhancing the robustness of the controllers obtained in the previous stage by redesigning the gain matrices. The worst-case parametric configuration that causes the peak observed in the SSV plots can be retrieved using MATLAB functions, such as wcgain or robstab. This worst-case model is then appended to the array of 71 models that was used for the first design, and the systune function is called a second time. Adding the destabilising configuration to the set of design models forces the new gains to not only stabilise the faulty configuration, but also enforce the tuning goals for all 71+1 design models. The redesign was performed for both halves of the flight envelope, considering the worst-case model at median speeds. Table 2 lists $\gamma_H$ and $\gamma_S$ after the second call. Their values show that the hard objectives, and not the soft ones, are met, which is the expected result. SSV analysis was performed for the newly obtained sets of gains under the same conditions as those used for the first set. The plots for the 35 kts uncertain model are shown in Fig. 4b. In this case, the peak value is extremely close to 1, which means that robust stability is guaranteed for the level of uncertainty defined when building the uncertain helicopter model. The multi-model approach enabled a design that is 3.5 times more robust at 35 kts without downgrading the performance. At 105 kts, robust stability is guaranteed for 116% of the uncertainty range after the second step. However, the SSV analysis was performed at the two median speeds only. Thus, the question remains as to whether the procedure should be repeated for every design speed, which would be extremely time consuming. To explore this issue further, the peak values of the $\mu$ upper bound were plotted for the entire speed range after the first and second calls to systune, as shown in Fig. 5. The discontinuity observed at 70 kts can be attributed to the fact that the low- and high-speed controllers were designed separately. Therefore, enforcing continuous level of robust stability over the entire flight envelope is difficult. Moreover,

**Table 2** $\gamma_H$ and $\gamma_S$ after the second call

| Speed range (kts) | $\gamma_H$ | $\gamma_S$ |
|---|---|---|
| 0-70 | 0.997 | 2.4102 |
| 70-140 | 0.9995 | 1.829 |

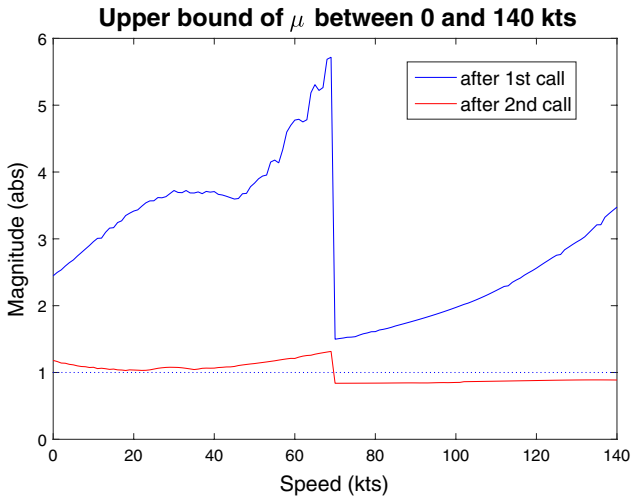


**Fig. 5** Peak value of the $\mu$ upper bound as a function of airspeed

the plots reveal that repetition of SSV analysis at every design point is unnecessary. The robustness of the controller improved significantly over the entire speed range after the second call, although the gain matrices were recomputed by considering only the destabilising configurations at 35 and 105 kts. For speeds higher than 70 kts, the upper bound is lower than 1, which indicates that the robustness cannot be further improved by following the introduced procedure. Nevertheless, the function can be called a third time to improve the robustness below 70 kts by considering the destabilising configurations in hover and near 70 kts. The next section analyses the results observed using the sets of gains obtained after the second call.

## 4 Results analysis

In this section, the performance delivered by the obtained ACAH system is compared with the design objectives. Subsequently, the HQ are assessed with respect to the selected ADS-33 criteria.

### 4.1 Tuning goals checklist

#### 4.1.1 Tracking requirement

Figure 6 shows the responses of the attitude angles to a unit step input on each channel and for all design points between 0 and 140 kts. A total of $9 \times 141$ time histories are therefore presented in the figure, which also shows the theoretical responses of the reference models. As can be seen, all time histories remain close to the targets defined by the reference models. This indicates that the combination of the reference model tracking and multi-model approaches leads to a consistent response of the flight control system in the time domain throughout the flight envelope. Moreover, the time histories exhibit good inter-axis decoupling, which is also a consequence of the selected approach. Despite the absence of tuning goals directly associated with decoupling requirements, the tracking mismatch tolerance used along with Step Tracking retains the off-axis responses within the prescribed mismatch limits. Therefore, this tolerance can be used as a tuning knob for inter-axis decoupling. In other words, specifying tighter tolerances improves the decoupling. However, the risk remains that either actuator saturation will occur or the optimisation problem will become impossible for the systune function to solve.

The time histories shown in Fig. 6 were obtained using the nominal representation of the helicopter dynamics between 0 and 140 kts. It is worth investigating how the system behaves when faced with the parametric uncertainties introduced in subsection 3.3.2. According to the SSV analysis, robust stability is guaranteed for the level of uncertainty that was defined; however, no conclusion can be drawn about robust performance. In other words, the flight control system will remain stable for any parametric configuration within the defined range, and yet its response to inputs might become unacceptable. To investigate this issue, the worst-case configurations at 35 and 105 kts were retrieved. Figure 7 shows the step responses of the designed controllers when operating under the nominal and worst-case conditions. As can be seen, the worst-case responses in pitch and yaw remained extremely close to those obtained using the nominal model. On the roll axis, the time histories slightly deteriorated in comparison with those obtained

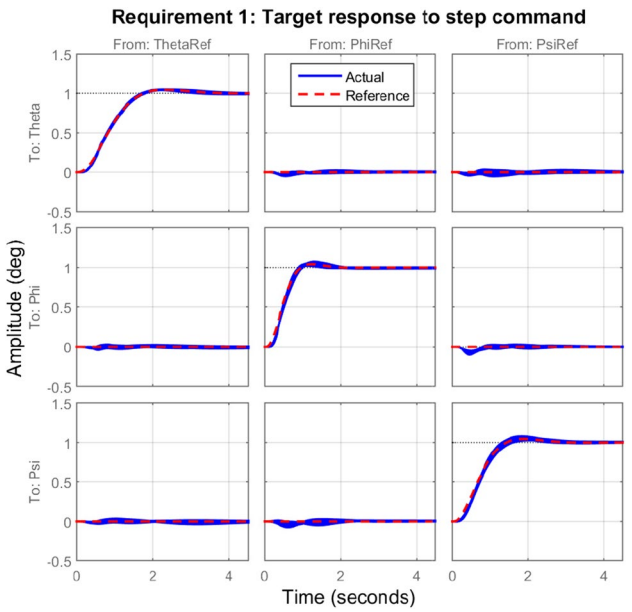


**Fig. 6** Unit step responses of the ACAH system (solid) and reference models (dashed)

in the nominal configuration. The worst-case responses remained, however, acceptable.

#### 4.1.2 Stability margins requirement

Figure 8 shows the disk-based gain and phase margins as functions of frequency for each axis and at 141 different speeds. The minimum gain margins are approximately 8 dB on all axes, which is well above the 6 dB objective. In contrast, the minimum phase margins are just higher than the 45° target on all axes, which explains why $\gamma_H$ is lower than, but extremely close to 1. This effect is a consequence of using a combination of hard and soft requirements. The systune function fulfilled the minimum phase margin hard objective. Thus, the remaining degrees of freedom could be dedicated to meeting the soft objective.

Figure 9 shows the classical and disk-based stability margins across the entire speed range. The curves suggest that the disk-based gain and phase margins are tightly correlated, unlike the classical margins. Further insight into this finding can be gained considering the relationship between the disk-based gain and phase margins [12]. Using the notations of Fig. 2, the abscissa c of the center C and the radius r of the disk are given in Eq. (6)

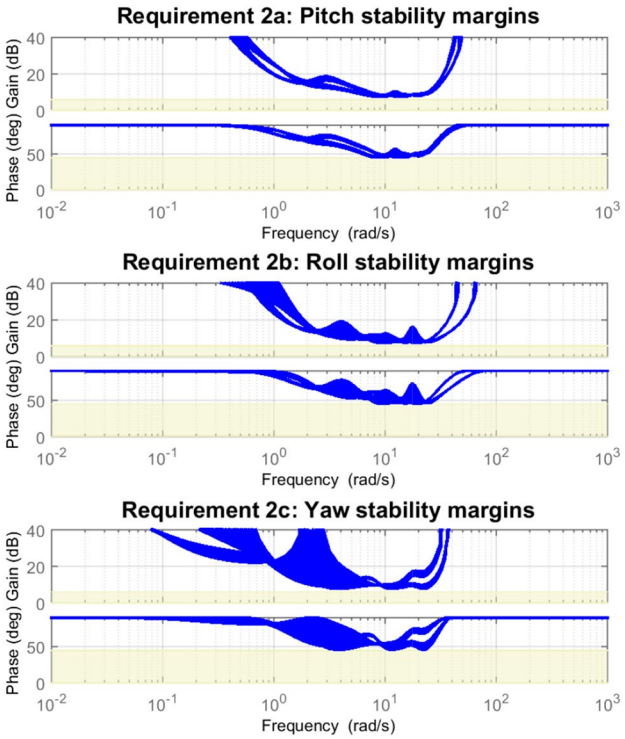


**Fig. 8** Gain and phase disk-based margins

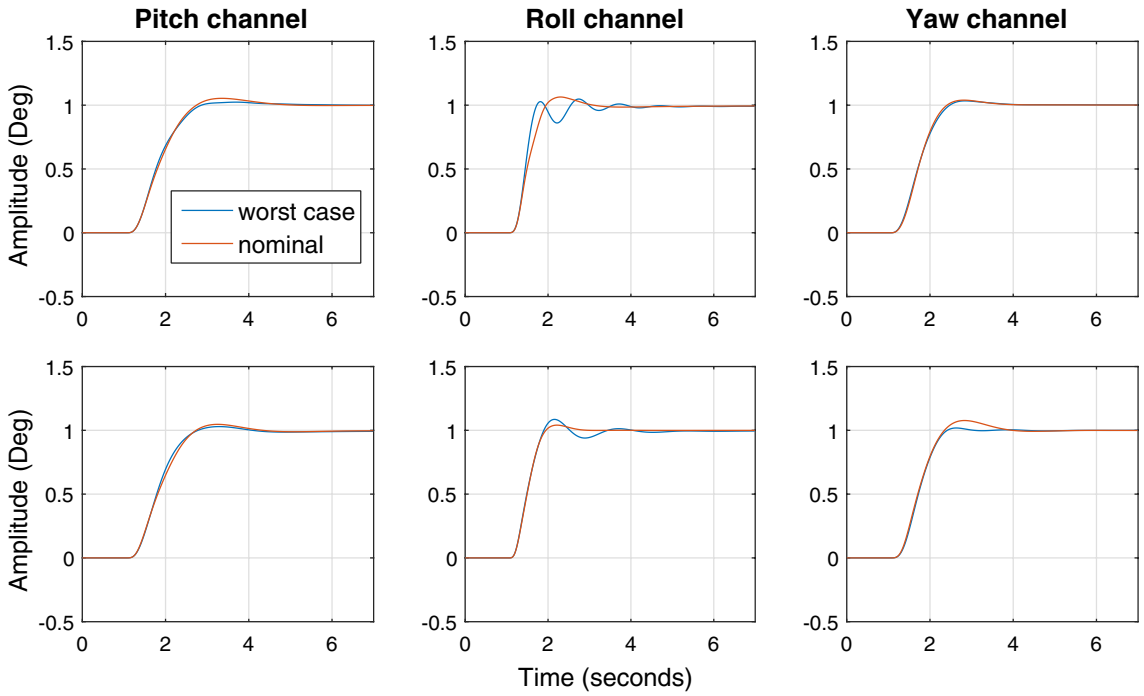


**Fig. 7** Worst-case and nominal step responses on each channel, at 35 kts (top row) and 105 kts (bottom row)

$$\begin{cases} c = \dfrac{\gamma + \gamma^{-1}}{2} = \dfrac{\gamma^2 + 1}{2\gamma} \\ r = \dfrac{\gamma - \gamma^{-1}}{2} = \dfrac{\gamma^2 - 1}{2\gamma} \end{cases} \tag{6}$$

Furthermore, the disk intersects the unit circle at $A = cos\phi_d + jsin\phi_d$. In the balanced case, triangle OAC is square and therefore: $sin\phi_d = \frac{r}{c}$. Using the expressions of r and c in Eq. (6), one finds the equation relating $\phi_d$ and $\gamma$:

$$sin\phi_d = \frac{\gamma^2 - 1}{\gamma^2 + 1} \tag{7}$$

This equation demonstrates that the disk-based gain and phase margins are not independent. Thus, if the desired minimum phase margin is set to 45°, solving Eq. (7) for $\gamma$ yields a minimum gain margin of $1 + \sqrt{2}$ (i.e. ± 7.65 dB), which is consistent with the data reported in Fig. 9. Therefore, the 45° phase margin objective implicitely contained the 6 dB gain requirement. In addition, Fig. 9 illustrates the relationships between the classical and disk-based margins as described in Eq. (5). The case of the yaw channel phase margins is particularly noteworthy. The classical and disk-based margins are almost equal between 70 and 88 kts. In contrast, they follow opposite trends between 88 and 140 kts. At 140 kts, the classical phase margin is more than 20° higher than the disk-based margin.

Furthermore, like the classical margins, the stability objectives specified by the Margins tuning goal are loop-at-a-time margins. Perturbations are considered in the loop under scrutiny while the other loops are supposed to operate under nominal conditions. However, gain and phase perturbations are likely to affect all loops simultaneously during real operation. Two different types of multiloop disk margins can be computed to account for simultaneous perturbations in all feedback channels. The first type considers simultaneous gain and phase variations in all channels, at either plant input or plant output. The second type is even more stringent because it considers simultaneous gain and phase variations in all channels, at both input and output. Multiloop margins provide a more realistic assessment of the system stability margins. They are, however, significantly lower than the loop-at-a-time disk margins, as can be observed in Fig. 10. As a conclusion, the advantages of the Margins tuning goal are twofold. First, the stability objectives are easily and consistently enforced throughout the entire speed range. Second, simultaneous gain and phase variations are considered, unlike the classical margins. However, the disk margins can be seen more as a complement than an alternative to the classical margins. Combining the latter with the loop-at-a-time and multiloop disk margins provides a more comprehensive insight into the system stability throughout the flight envelope.

#### 4.1.3 Gain limitation requirements

The transfers mentioned in section 3.2.3 are plotted in Fig. 11 at 141 speeds against their respective limits. As can be seen, the two hard requirements (3a and 3b) could be just satisfied as the magnitudes of the gains very closely approach the boundaries defined by $W_1$ and $W_2$. The value of

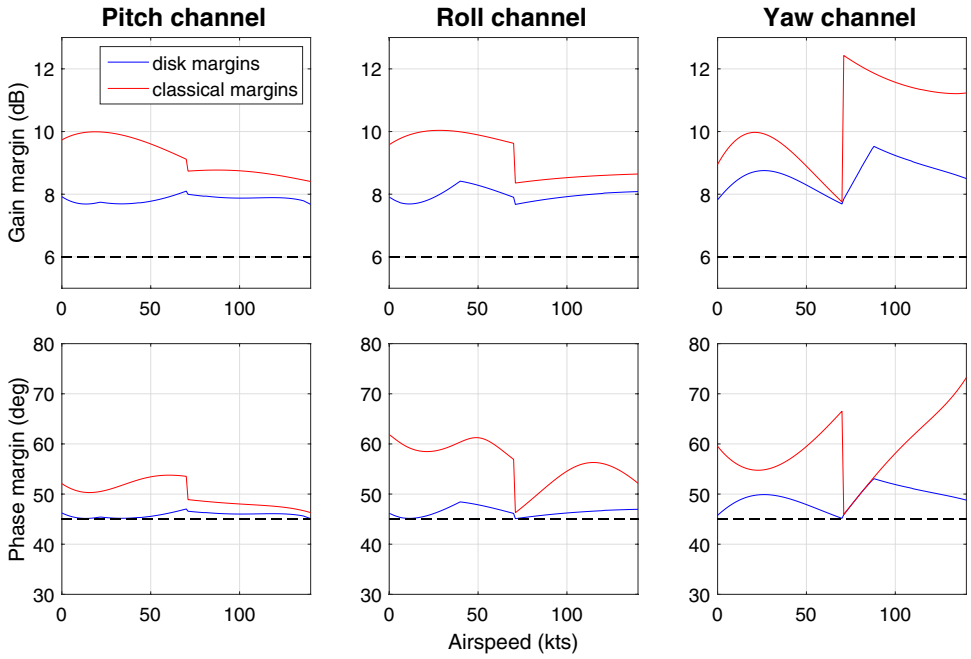


**Fig. 9** Classical and disk-based margins throughout the flight envelope

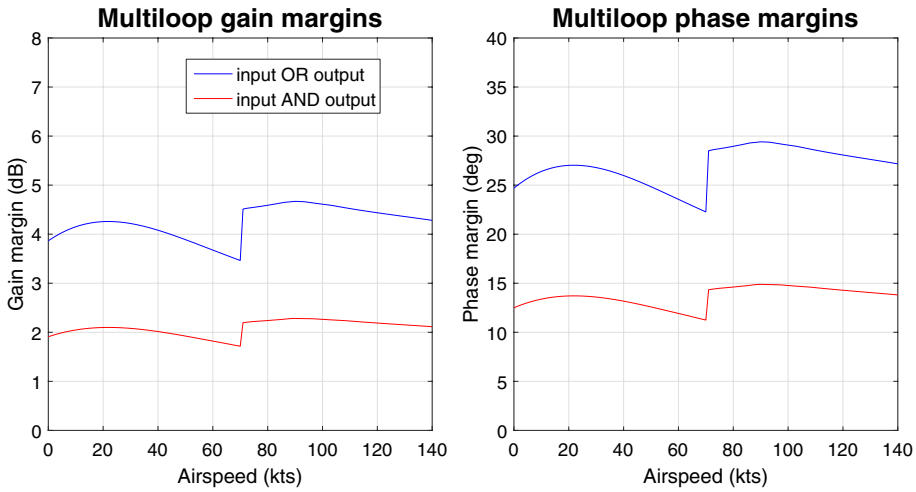


**Fig. 10** Multiloop disk margins with perturbations at input or output, and simultaneously at both input and output

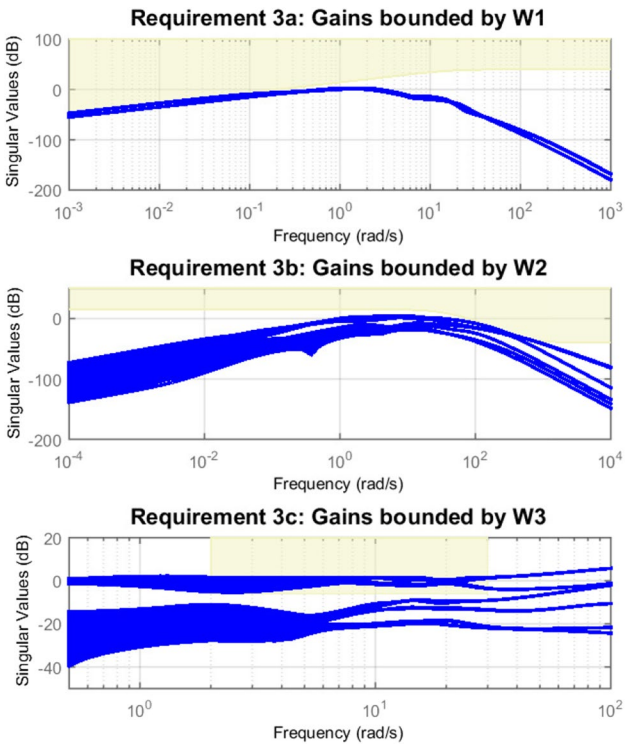


**Fig. 11** Gain magnitudes

$\gamma_S$ indicated that the soft requirement could not be satisfied, which is confirmed by the plot of requirement 3c at the bottom of the figure: the limit defined by $W_3$ could not be enforced for all gains at all speeds. Further analysis indicates that the limit is exceeded by $T_{\psi_{ref}\to\delta_\psi}$ at all speeds, whereas $T_{\theta_{ref}\to\delta_\theta}$ and $T_{\varphi_{ref}\to\delta_\varphi}$ always remain below the prescribed boundary.

In addition, the effects of the "Gain" goals in the time domain can be evaluated by comparing the proposed design with a controller that was obtained using all but the "Gain" goals. The effects of this tuning goal on actuator activity are particularly noteworthy on the yaw axis. Figure 12 shows the tail rotor actuator speed $\dot{\delta}_{ped}$ and yaw angle $\psi$ responses to unit step inputs on all axes, obtained in hover with either design. The responses to the $\theta$, $\varphi$ and $\psi$ steps show that both designs deliver comparable performances in terms of reference tracking and disturbance rejection when the use of the Gain goal significantly reduces actuator activity. The response to collective input demonstrates the conflicting influence of $W_1$ and $W_2$ at medium frequencies. Although efficient disturbance rejection requires prompt reaction from the actuators, robustness requires limiting their activity at higher frequencies. $W_1$ and $W_2$ can, therefore, be used as tuning degrees of freedom to establish the desired compromise between these competing objectives. In this example, the activity of the actuator was reduced at the cost of collective input disturbance rejection.

## 4.2 Handling qualities assessment

In this subsection, the performance of the resulting design is evaluated against the attitude quickness, bandwidth and inter-axis coupling ADS-33 criteria. The analyses were performed at eight different speeds spanning the entire speed range.

### 4.2.1 Attitude quickness

This criterion is defined by ADS-33 and uses moderate-amplitude step inputs to assess the agility of the helicopter along each axis. The parameter under scrutiny is the ratio of the peak angular rate to the peak attitude change. Figure 13 shows the results obtained using the designed system for the three axes, which can be compared with the theoretical performance of the reference models. The pitch and yaw

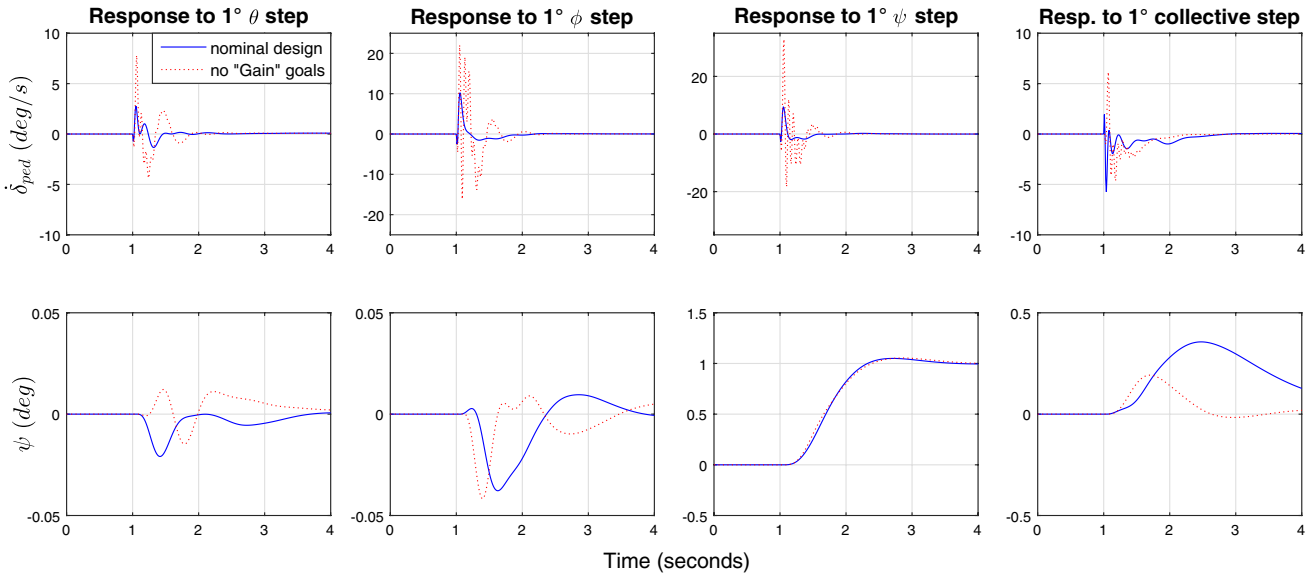


**Fig. 12** Responses of the tail rotor actuator speed and yaw angle to unit step inputs (0 kt)

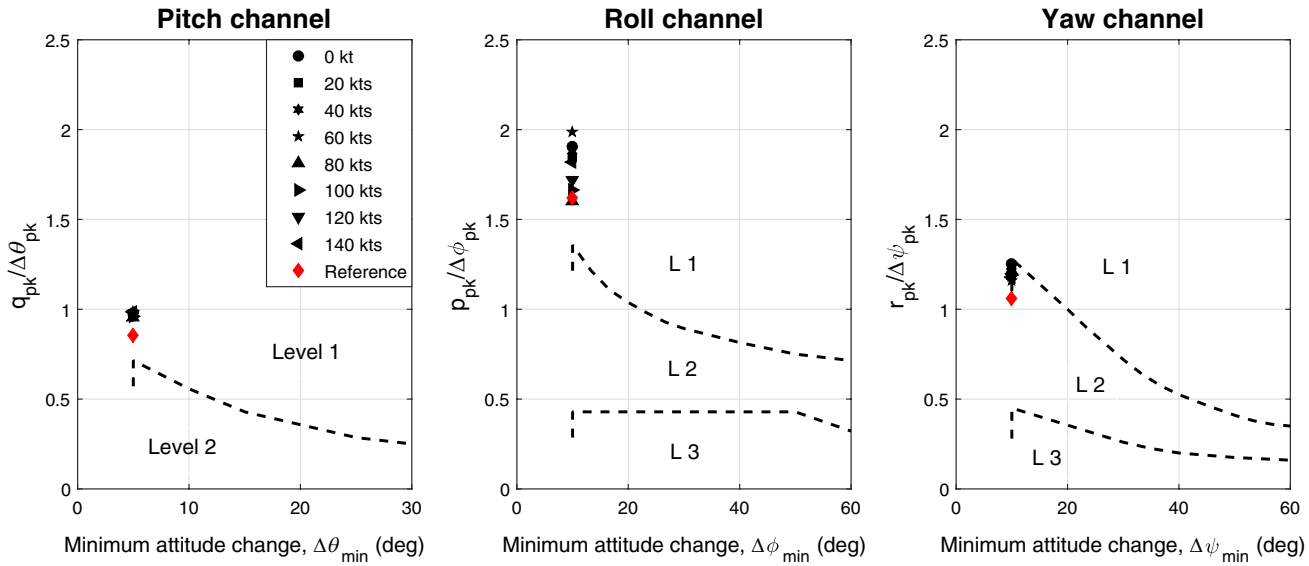


**Fig. 13** Requirements for moderate-amplitude pitch, roll and heading attitude changes (All Other MTEs)

channels exhibit very consistent results over the entire speed range, whereas greater dispersion can be observed on the roll channel. Depending on the speed and axis, the designed system either meets or surpasses the targets set by the reference models.

This finding can be investigated by analysing the roll response at 60 kts, for which the discrepancy between the reference model and the actual system is the largest. The ratio between the peak roll rate and peak angle is 1.99 for the actual system, and only 1.62 for the reference model. Figure 14 shows the roll attitude frequency response for the reference model and actual system at 60 kts. As observed, beyond 10 rad/s, the magnitude of the actual design rolls off faster than that of the reference model, which is one of the effects of the Gain tuning goal. This explains, along with the digital delay in the closed loop, why the initial response of the actual system is slower than that of the reference model, as shown in Fig. 15. However, the Step Tracking goal still imposes tight tracking of the reference model. Therefore, the higher peak roll rate in the actual design response compensates for the slower initial response. In contrast to the peak roll rates, the peak roll angles are almost equal, which

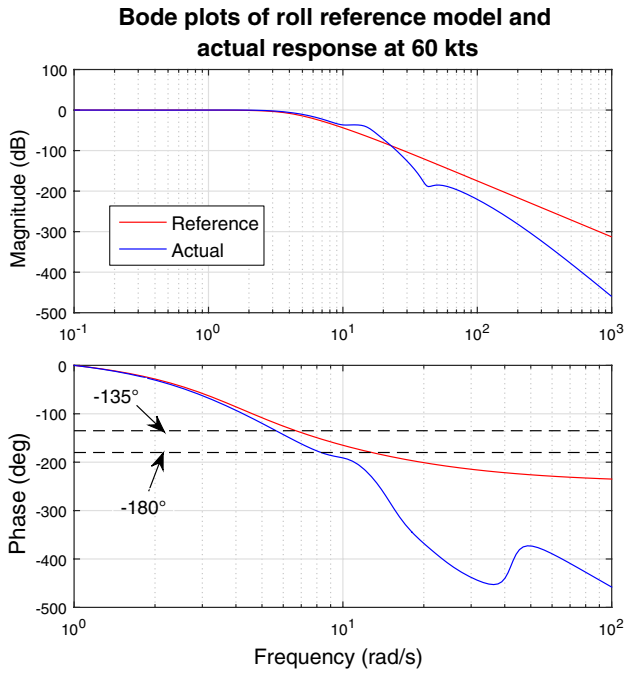


**Fig. 14** Bode plots of the roll attitude response (reference model and actual system)

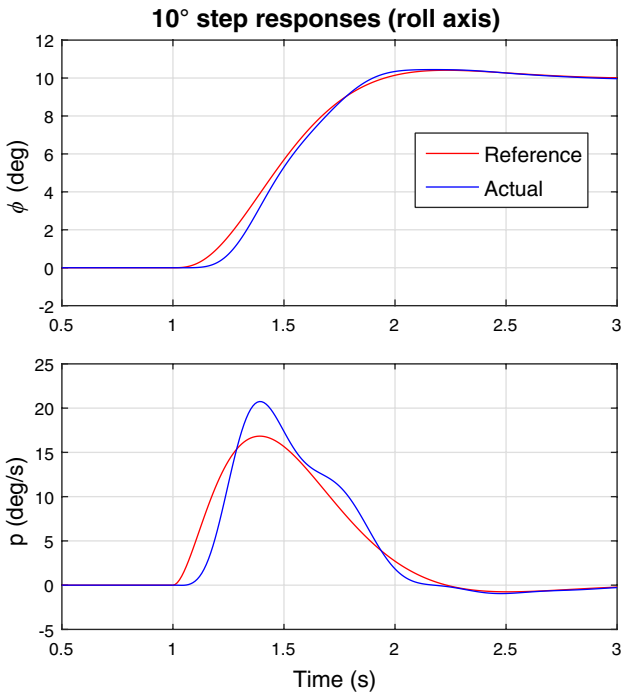


**Fig. 15** Responses to a roll step input of the reference model and actual system at 60 kts

explains the observed ratio discrepancy. Once again, the systune function had to compromise between the conflicting objectives imposed by the Gain and Step Tracking goals. The dispersion observed on the roll channel can be mitigated by specifying a tighter reference tracking margin. The constraints of the Gain goal would then have to be relaxed; otherwise, the optimisation problem might become infeasible. Although the systune function is designed to determine the optimal solution for a given set of constraints, engineers remain responsible for establishing the design tradeoffs by properly selecting the tuning objectives.

#### 4.2.2 Bandwidth

This ADS-33 criterion assesses the accuracy of control input tracking in the frequency domain using two parameters: phase delay and bandwidth frequency. The latter is defined for ACAH response types as the frequency at which the phase is – 135°. The phase delay $\tau_p$ is defined according to Eq. (8).

$$\tau_p = \frac{\Delta\Phi_{2\omega_{180}}}{57.3\ (2\omega_{180})} \tag{8}$$

where $\omega_{180}$ is the frequency at which the phase is – 180°, and $\Delta\Phi_{2\omega_{180}}$ is the phase shift between frequencies $\omega_{180}$ and $2 \times \omega_{180}$. Figure 16 shows the application of this criterion to the designed flight control system and reference models.

Level 1 performance is achieved at all speeds and for the three axes. On the pitch axis, the bandwidth is consistent with that of the reference model, whereas this parameter is up to 0.5 rad/s lower than expected on the roll and yaw axes. This discrepancy can be attributed to the quicker drop-off that the Gain goal also induces on the phase curve, as can be seen in Fig. 14. Similarly, the observed phase delays are higher than those of the reference models. Owing to the steeper phase drop-off, the $\omega_{180}$ frequency of the actual design is lower than that of the reference, and the phase shift $\Delta\Phi_{2\omega_{180}}$ is higher. Consequently, according to the definition given in Eq. (8), the phase delay observed in the case of the actual design is higher than that of the reference models. This is another example of the design compromises that must be made.

#### 4.2.3 Inter-axis coupling

Helicopters are strongly coupled aircraft, and ADS-33 quantifies the pitch-due-to-roll and roll-due-to-pitch coupling for aggressive agility as follows [3]: "The ratio of peak off-axis attitude response from trim within 4 s to the desired (on-axis) attitude response from trim at 4 s, $\Delta\theta_{pk}$ / $\Delta\phi_4$ ($\Delta\phi_{pk}$ / $\Delta\theta_4$), following an abrupt lateral (longitudinal) cockpit control step input, shall not exceed ± 0.25 for Level 1 or ± 0.60 for Level 2. Heading shall be maintained essentially constant." As observed in Fig. 6, the designed system easily meets the Level 1 requirements. The guidelines also

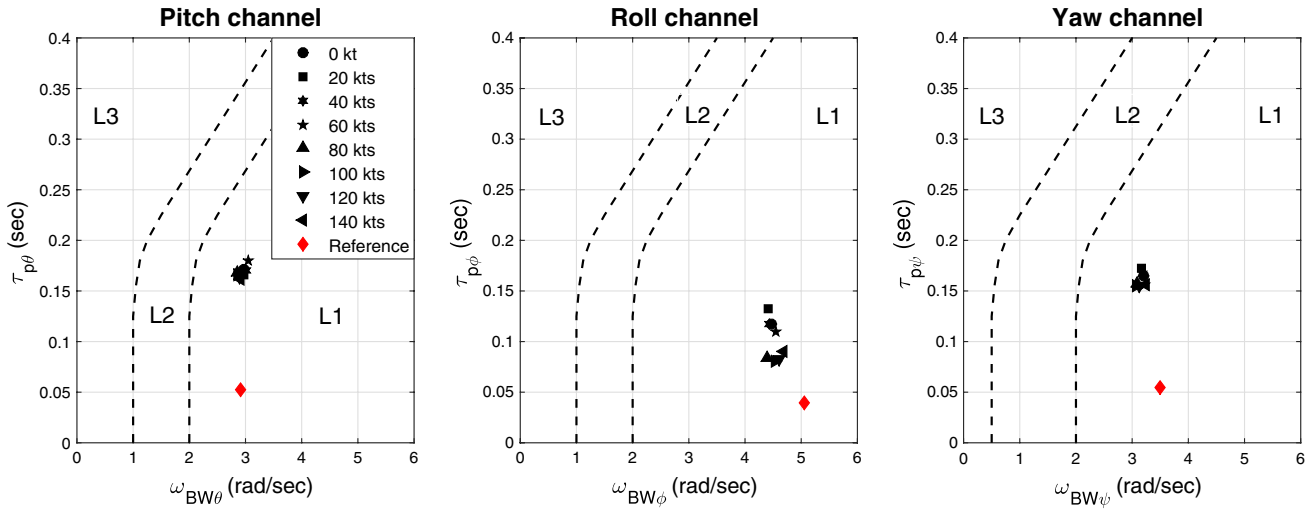


**Fig. 16** Bandwidth requirements for small-amplitude attitude changes (All other MTEs - UCE > 1 and/or Divided Attention operations)

specify more stringent requirements for "Target Acquisition and Tracking", which are defined in the frequency domain and typically apply to combat helicopters. Based on this criterion, the proposed design achieves Level 2 performance at 20 kts, and Level 1 performance at all other speeds, as shown in Fig. 17.

The rejection of the disturbances caused by collective inputs on the pitch, roll and yaw axes is assessed using the time histories shown in Fig. 18, although it is not an ADS-33 criterion. The figure presents the off-axis responses to a 1° collective input at 141 speeds between hover and 140 kts. The quality of the disturbance rejection observed in this figure is the result of the design compromise established using profiles $W_1$ and $W_2$. However, faster and more efficient decoupling could have been achieved by tightening the constraints imposed by $W_1$ and/or relaxing those specified by $W_2$, at the cost of higher actuator activity. In addition, the time histories of each axis are broken into two groups. Each of these corresponds to a specific set of gain matrices, and the time responses are consistent within each half of the flight envelope. However, enforcing this consistency over the entire speed range was not possible.

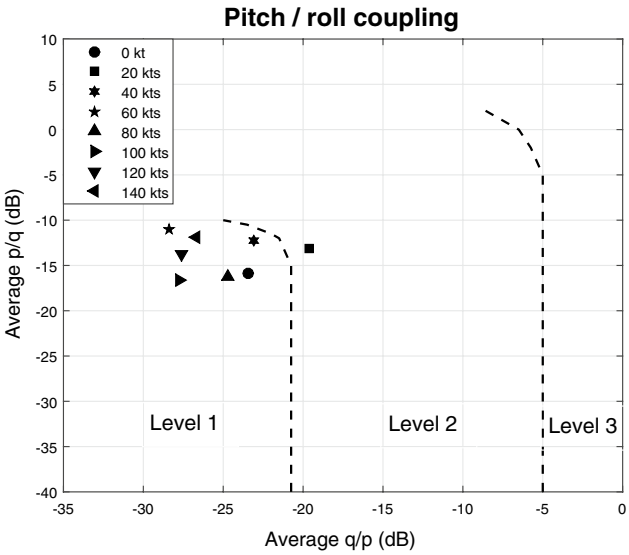


**Fig. 17** Requirements for pitch-due-to-roll and roll-due-to-pitch (Target Acquisition and Tracking)

## 5 Conclusion

Despite significant advances in different fields, such as aerodynamics, system identification and control theory, designing rotorcraft flight control laws remains an arduous and time-consuming task. The major problems include strong inter-axis coupling, unmodeled rotor dynamics and nonlinear effects. Furthermore, connecting the HQ objectives and design methodology is challenging. Thus, this study introduced an innovative flight control architecture and design methodology. In the proposed architecture, the usual PID-based arrangement is replaced with a single dynamic controller, and the collective axis is considered; the design methodology adopts the multi-objective and multi-model approaches.

The proposed methodology introduces several advantages to the design process. First, the use of a single controller simplifies the system architecture. Furthermore, considering all axes simultaneously mitigates undesired couplings without the need for additional inter-axis decoupling gains. The use of reference models with the Step Tracking goal helps predict the level of performance of the design when the Gain objectives limit the response of the system at high

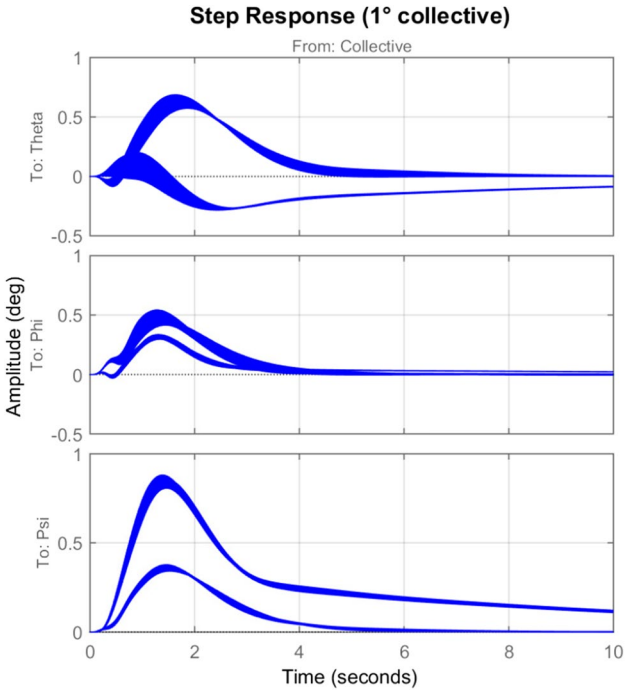


**Fig. 18** Pitch, roll and yaw responses to collective step

frequencies and establish a compromise between performance and robustness. The multi-model approach reduces the effort required in the design, because it ensures that two sets of controller gains are sufficient to address the entire speed range. This approach also guarantees that the gain and phase margins are enforced throughout the flight envelope. Furthermore, $\mu$-analysis can be used in conjunction with the multi-model approach to enhance the robustness of the design against parametric uncertainties.

However, this methodology also has drawbacks. Finding the right settings for design parameters, such as the gain limitation profiles or the value of $\beta$ in Eq. (2), is an iterative and time-consuming process that relies on the designer's experience. In addition, the different design objectives specified using the tuning goals have conflicting effects, which might hamper the accurate prediction of HQ with respect to certain criteria such as attitude quickness or phase delay. Furthermore, the rotorcraft industry might be reluctant, for various reasons, to adopt a design that significantly differs from the conventional one.

Nevertheless, the proposed methodology deserves further attention. The resulting flight control system not only possesses interesting performance and robustness properties but also simplifies the design process, despite the aforementioned drawbacks. Future works could aim at establishing guidelines to facilitate design compromises. In particular, further effort is required to better understand the connections between frequency-domain tuning goals and observed handling qualities. In addition, the next steps may also include testing the designed controller against a high-fidelity nonlinear model of the helicopter to confirm the positive results that were obtained applying the selected ADS-33 criteria to the linear model. Indeed, a comprehensive validation of the flight control system must account for nonlinear phenomena such as the dynamics of the aircraft, or actuator authority and rate limit constraints. Furthermore, owing to the multi-model approach, only two sets of gains are sufficient to address the entire speed range. This robustness against plant variations will be put to the test by the nonlinear model.

**Data availability** Not applicable.

## Declarations

**Conflict of interest** The author has no competing interests to declare that are relevant to the content of this article. No funding was received for conducting this study.

## References

1. Stiles, L.R., Mayo, J., Freisner, A.L., Landis, K.H., and Kothmann, B.D.: Impossible to Resist: The Development of Rotorcraft Fly-by-Wire Technology. In American Helicopter Society $60^{th}$ Annual Forum (2004)
2. Huo, J., Gu, H.: Survey on flight control technology for large-scale helicopter. Int. J. Aerosp. Eng. **2017**(02), 1–14 (2017)
3. Anonymous.: Aeronautical Design Standard - Performance Specification. Handling Qualities Requirements for Military Rotorcraft ADS-33E-PRF, March (2000)
4. Tischler, M., Colbourne, J., Morel, M., Biezad, D., Levine, W., Moldoveanu, V.: CONDUIT: a new multidisciplinary integration environment for flight control development (1997)
5. Antonioli, J.C., Taghizad, A., Rakotomamonjy, T., Ouladsine, M.: Helicopter flight control design tool integrating handling qualities. In $5^{th}$ European Conference for Aerospace Sciences (EUCASS) (2013)
6. Antonioli, J.C., Taghizad, A., Rakotomamonjy, T., Ouladsine, M.: Development of flying qualities based charts as a support for the initialization of the gains of helicopter control laws. In IEEE Conference on Control Applications (CCA/MSC) (2014)
7. Antonioli, J.C., Taghizad, A., Rakotomamonjy, T., Ouladsine, M.: Towards the development of a methodology for designing helicopter flight control laws by integrating handling qualities requirements from the first stage of tuning. In $40^{th}$ European Rotorcraft Forum (ERF) (2014)
8. Biannic, J.-M., Taghizad, A., Dujols, L., Perozzi, G.: A multiobjective $H_\infty$ design framewok for helicopter PID control tuning with handling qualities requirements. In $7^{th}$ European Conference for Aerospace Sciences (EUCASS) (2017)
9. Srinathkumar, S.: Eigenstructure control: a rotorcraft handling qualities engineering tool. J. Am. Helicopter Soc. **60**, 04 (2015)
10. Padfield, G.D.: Helicopter flight dynamics, 2nd edn. Blackwell Publishing, Oxford (2007)

11. Srinathkumar, S.: Eigenstructure control algorithms, Applications to aircraft/rotorcraft handling qualities design, IET Control Engineering Series 74 (2011)
12. Seiler, P., Packard, A., Gahinet, P.: An introduction to disk margins. IEEE Control Syst. Mag. **40**, 10 (2020)
13. Apkarian, P., Noll, D.: Non-smooth $H_\infty$ synthesis. IEEE Trans. Autom. Control **51**(1), 229–244 (2006)
14. Gahinet, P., Apkarian, P.: Structured H-Infinity Synthesis in MATLAB. In IFAC Proceedings Volumes (IFAC-PapersOnline), 18, 1435–1440 (2011)
15. Apkarian, P., Gahinet, P., Buhr, C.: Multi-model, multi-objective tuning of fixed-structure controllers. In European Control Conference (ECC) Proceedings, 856–861 (2014)
16. Apkarian, P., Dao, M.-N., Noll, D.: Parametric robust structured control design. IEEE Trans. Autom. Control **60**(7), 1857–1869 (2015)